Growth of Oxygen Precipitates and Dislocations in Czochralski Silicon

Fiacre E. Rougieux, *Member, IEEE*, Hieu T. Nguyen, Daniel H. Macdonald, *Senior Member, IEEE*, Bernhard Mitchell, and Robert Falster

***Abstract*—The impact of oxygen precipitates and dislocations on carrier recombination is investigated on thick silicon slabs cut vertically from a Czochralski-grown silicon ingot. Using a combination of photoluminescence imaging, photoluminescence spectroscopy, and Fourier transform infrared spectroscopy, we investigate the impact of pre-anneal on their recombination activity. We show that the vacancy concentration during precipitate growth affects the recombination activity of oxygen precipitates. Finally, we demonstrate the impact of nonequilibrium point defect concentrations on precipitate and dislocation growth.**

***Index Terms*—Czochralski, dislocations, Fourier transform infrared spectroscopy (FTIR), minority carrier lifetime, oxygen precipitates, photoluminescence, self-interstitials, silicon, vacancy.**

I. Introduction

OXYGEN precipitates are recombination active in silicon and reduce the minority carrier lifetime and the efficiency in silicon solar cells [1]–[11]. Additionally, oxygen precipitation is often spatially nonhomogeneous, leading to the formation of disc- or ring-like structures [1], [3], [6], [8], [11]. Oxygen precipitation leads to a significant volume expansion with an associated strain. This strain is released via the absorption of silicon vacancies or emission of silicon self-interstitials. Evidently vacancy-rich silicon will tend to promote oxygen precipitation and growth while interstitial-rich silicon will tend to slow oxygen precipitation and growth but promote dislocation growth [12], [13]. Upon heating to 1100 °C, vacancies and interstitials are generated in equal concentrations through Frenkel-pair generation. A nitrogen ambient also leads to vacancy surface generation [14]–[19], while an oxygen ambient leads to interstitial surface generation [17], [18], [20]. Through controlled annealing one can thus explore the creation of extended defects in vacancy-rich and interstitial-rich environments, and their relative impact on the minority carrier lifetime.

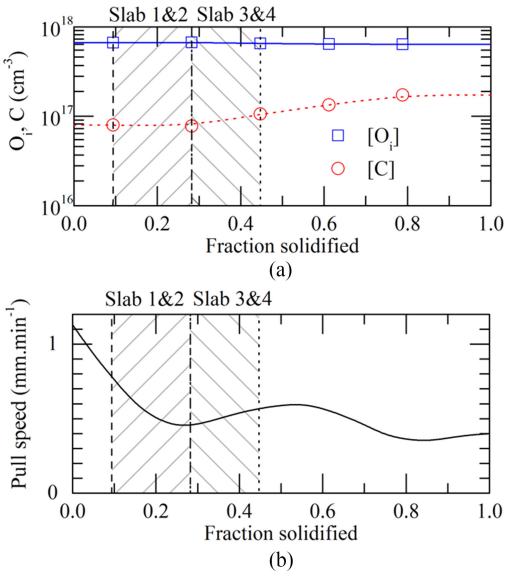

Fig. 1. (a) Oxygen and carbon concentrations as a function of solidified fraction. (b) Pull speed as a function of solidified fraction, the position of slabs 1–4 is also shown.

In this paper, we perform tabula rasa treatments followed by two-step anneal treatments in order to examine the impact of dislocations and oxygen precipitates on the minority carrier lifetime. We show that at similar precipitated concentration, the recombination activity of precipitates is significantly increased in vacancy-rich silicon. Finally, our results indicate that the cooldown rate after annealing may lead to out-of-equilibrium intrinsic point defect concentrations that contribute to the growth of oxygen precipitates or the formation of dislocations during subsequent processing.

II. Experimental Methods

The slabs used in this study were 2 mm thick vertical cuts from the center of a 200 mm diameter boron doped n-type Czochralski silicon ingot. The resistivity varied from 9.3 to 13.3 $\Omega \cdot$ cm. The oxygen and carbon concentrations are shown in Fig. 1(a). In order to study both vacancy-rich and interstitial-rich regions, the ingot pulling speed was varied between 1.2 and 0.3 mm $\cdot$ min^{-1}. The pulling speed profile is shown in Fig. 1(b). The slabs were 14 cm long and 20 cm

Manuscript received January 12, 2017; revised February 16, 2017; accepted February 21, 2017. This work was supported in part by the Australian Research Council through a Discovery Early Career Researcher Award and in part by the Australian Renewable Energy Agency through project RND009.

F. E. Rougieux, H. T. Nguyen, and D. H. Macdonald are with the Research School of Engineering, College of Engineering and Computer Science, Australian National University, Canberra, ACT 0200, Australia (e-mail: fiacre.rougieux@anu.edu.au; hieu.nguyen@anu.edu.au; daniel.macdonald@anu.edu.au).

B. Mitchell is with the School of Photovoltaic and Renewable Energy Engineering, University of New South Wales, Sydney, NSW 2052, Australia (e-mail: bernhard.mitchell@unsw.edu.au).

R. Falster is with SunEdison Semiconductor, Merano 39012, Italy (e-mail: rfalster@btinternet.com).

Color versions of one or more of the figures in this paper are available online at http://ieeexplore.ieee.org

Digital Object Identifier 10.1109/JPHOTOV.2017.2678840

wide. Slabs 1 and 2 were sister slabs (adjacent), and slabs 3 and 4 were sister slabs, and to a large degree were mirror images of slabs 1 and 2, in terms of the variation in growth rate. The positions of slabs 1–4 are shown in Fig. 1.

All slabs were chemically etched to remove saw damage. Slabs 1 and 3 were decorated with Cu as described in [21]. The lifetime was measured with microwave photoconductance decay (PCD) and an optical image was taken after a Yang etch [22], [23]. This preparation allows for the delineation of vacancy- and interstitial-rich regions.

As the as-grown point defect distribution is symmetrical around the vertical growth axis, slabs 2 and 4 were cut in half. Slab 2A was kept in the as-cut state. To study the impact of ambient gas on a tabula rasa treatment, slab 2B was annealed at 1100 °C for 30 min in oxygen with a flow rate of $\sim 1501 \cdot h^{-1}$ and slab 4A at 1100 °C for 30 min in nitrogen also with a flow rate of $\sim 1501 \cdot h^{-1}$. The ramp up and cooldown rate was $\sim 20\,K \cdot min^{-1}$.

In order to understand oxygen precipitation during high temperature steps such as boron or phosphorus diffusion (800–950 °C), we performed a two-step anneal on all slabs (2A, 2B, and 4A). The two-step anneal consists of an anneal at 800 °C in nitrogen for 4 h followed by an anneal at 1000 °C in oxygen for 8 h. The 800 °C step simulates the thermal impact of a diffusion. Falster *et al.* have shown that this anneal does not lead to significant nucleation of oxygen precipitates, in fact some precipitates below a certain size dissolve [24]. However, the precipitates that survive grow in size (the distribution of precipitates size "drifts" to higher sizes) allowing them to survive the subsequent anneal at 1000 °C [24].

The subsequent anneal at 1000 °C leads to the growth of oxygen precipitates such that they become observable not only by lifetime spectroscopy, but also by Fourier transform infrared spectroscopy (FTIR), microphotoluminescence (μ-PL), and defect etch. This is a standard process for oxygen precipitate growth [25]. The calibration coefficients used for FTIR measurements were $2.45 \times 10^{17}\ cm^{-2}$ for oxygen and $8.1 \times 10^{16}\ cm^{-2}$ for carbon.

Note that carbon enhances oxygen precipitation. As shown in Fig. 1, the carbon concentration in our slabs is between [C] $= 8.0 \times 10^{16}$ and $1.8 \times 10^{17}\ cm^{-3}$ and as such it is likely to enhance precipitation (carbon provides centers for precipitate nucleation) [26]. Nevertheless, the slabs provide a good basis to study the impact of grown-in and process-induced defects on oxygen precipitates and dislocation generation.

Photoluminescence (PL) images were captured using a BT imaging tool [27]. Minority carrier lifetime measurements were performed using the Quasi Steady State Photoconductance (QSSPC) and transient photoconductance methods with a Sinton WCT120 system [28]. We used the thermal oxide grown during the two-step anneal as well as Plasma Enhanced Chemical Vapor Deposition (PECVD) silicon nitride for surface passivation (with J0-SiN $= 3.3\ fA \cdot cm^{-3}$). The measured lifetime was found to be the same with both films, but because the silicon nitride passivation featured surface scratches, we present only the thermally grown oxide passivated results for all PL images and spectroscopy measurements.

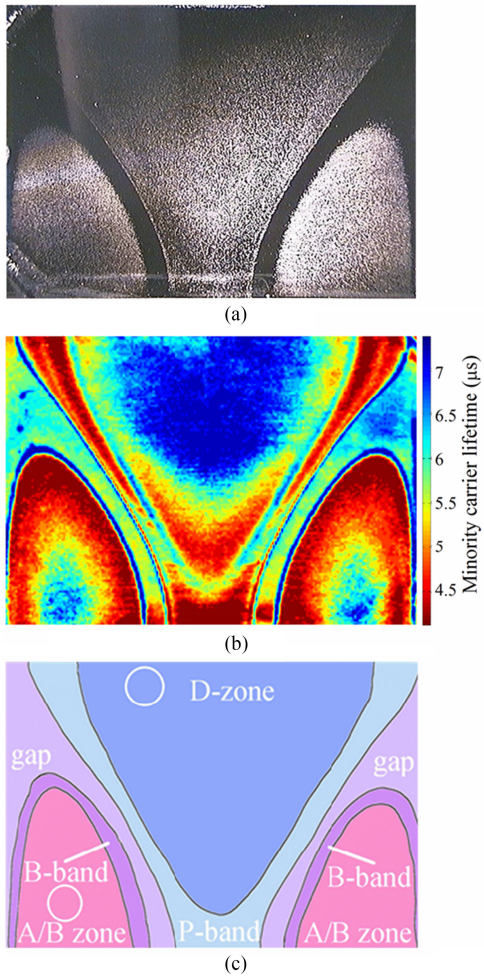

Fig. 2. Slab 1 (a) optical image of Cu-decorated slab, (b) microwave PCD image of the Cu-decorated slab, and (c) schematic spatial distribution of grown-in defects.

μ-PL spectroscopy measurements were conducted using a Horiba LabRam tool equipped with a confocal microscope and a liquid nitrogen cooled InGaAs array detector. An excitation wavelength of 810 nm was chosen in order to probe deeper than the immediate surface and the measurements were performed at 80 K. The excitation absorption depth at 80 K is $\sim 80\,\mu m$ [29]. For all measurements, a 50 × objective lens was used to focus the laser beam into a spot of 1.8 μm in diameter on the slabs. FTIR measurements were conducted using a Bruker Vertex 80 system with a resolution of $4\,cm^{-1}$.

III. Intrinsic Point Defect Distribution in Slabs

Fig. 2(a) shows the optical image of the Cu-decorated slab 1 after defect etch. The Cu-decorated image of slab 3 is similar to slab 1 (although flipped vertically) and is not shown here for brevity.

The inner vacancy-rich zone (D-zone) and outer interstitial-rich zone (A/B zone) are clearly visible [1]. The A/B zone is named after two types of swirl defects originally observed by defect etching and optical imaging, one large defect (A-swirl defect) and another smaller and more numerous defect

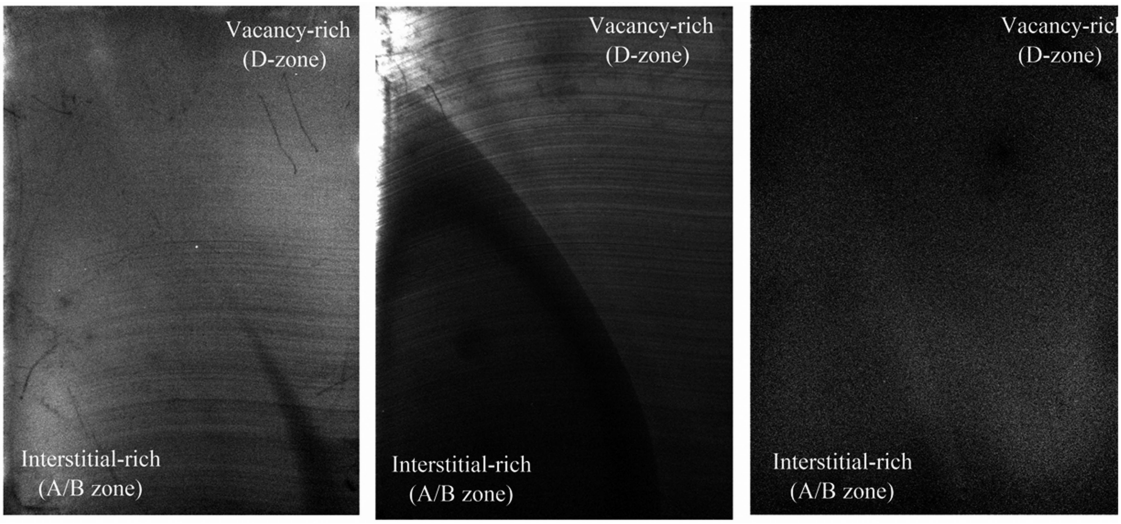

Fig. 3. Uncalibrated PL images after a two-step anneal for the (a) as-grown slab, (b) oxygen pre-annealed slab, and (c) nitrogen pre-annealed slab, after a two-step anneal. The contrast was adjusted allowing to see the features.

(B-swirl) [1]. The D-zone is named after another type of defect, D-defects (also named crystal-originated particles, light scattering tomography defects, or flow pattern defects). D-defects were originally observed by defect etching and consist of voids or vacancy aggregates [1].

The microwave PCD image in Fig. 2(b) reveals a more detailed structure showing the D-zone and A/B zone separated by the particle band (P-band), the gap, and the B-band [1]. The P-band is where numerous oxide particles are created during ingot cool-down, while the B-band is where B-swirls form [1]. In between, lies the gap, also called the perfect zone, a region where both vacancies and interstitials are in low concentration and where defect nucleation is not promoted [1]. For clarity, the different zones and bands are illustrated in Fig. 2(c).

IV. Oxygen Precipitates and Impact of Tabula Rasa

A. Minority Carrier Lifetime

The PL image of the lifetime after the two-step anneals is shown in Fig. 3. Noting that the slabs are relatively thick, the injection dependence is not included here, as it is affected by nonhomogeneous carrier profiles and the limited sense depth of the coil [30]–[32]. Indeed, a QSSCell simulation [33] shows that the carrier profile will vary by several orders of magnitudes across the 2 mm slab. In the slab not pre-annealed, the lifetime at $\Delta n = 1 \times 10^{14}\,\mathrm{cm}^{-3}$ is 2.5 μs in the interstitial-rich region and 2.0 μs in the vacancy-rich. In the pre-oxygen anneal slab, the lifetime at $\Delta n = 1 \times 10^{14}\,\mathrm{cm}^{-3}$ is 1.9 μs in the interstitial-rich region and 3.2 μs in the vacancy-rich region. In the prenitrogen annealed sample, the lifetime is not measurable. Note that the as-grown lifetime is higher than 500 μs and spatially homogeneous. This suggests that the lifetime before two-step anneal is not severely limited by the spatially nonuniform intrinsic point-defect distribution.

In the as-grown slab, the lifetime is homogeneously low in the slab after the two-step anneal, except for sections of the P-band, which are even lower. In the vacancy-rich region, void nucleation competes with oxygen precipitation. This means a lower density of oxygen precipitates form than in the P-band. The P-band has the lowest lifetime post the two-step anneal. This region is where the vacancy concentration is high but just below the concentration required for void nucleation [13]. This means during ingot cooling, vacancies are consumed by oxygen precipitates in this region [13]. These precipitates subsequently grow during the two-step anneal.

In the pre-oxidized slab, the lifetime is lower in the interstitial-rich region after the two-step anneal. The injection dependence of the lifetime is the same in both regions but shifted down for the interstitial-rich region. This could mean that the same defect is limiting the interstitial-rich region and the vacancy-rich region, with greater concentration in the interstitial-rich region. However, it is also possible that different defects limit both regions.

In the nitrogen annealed slab, the lifetime is homogeneously low and the injection dependence of the lifetime is not measureable. It appears that high concentrations of defects and/or defects with large capture cross-sections are present throughout the samples and reduce the minority-carrier lifetime to values not measurable (well below 1 μs).

B. Oxygen Reduction and Precipitation

Fig. 4 shows the FTIR spectra before and after the tabula rasa and two-step anneals. In the as-grown wafer [see Fig. 4(a)], there is little difference between the oxygen reduction in the vacancy-rich or the interstitial-rich regions after two-step annealing. This is in agreement with the minority carrier lifetime measurements showing little difference between the interstitial-rich region and vacancy-rich region; both are limited by the same amount of defects.

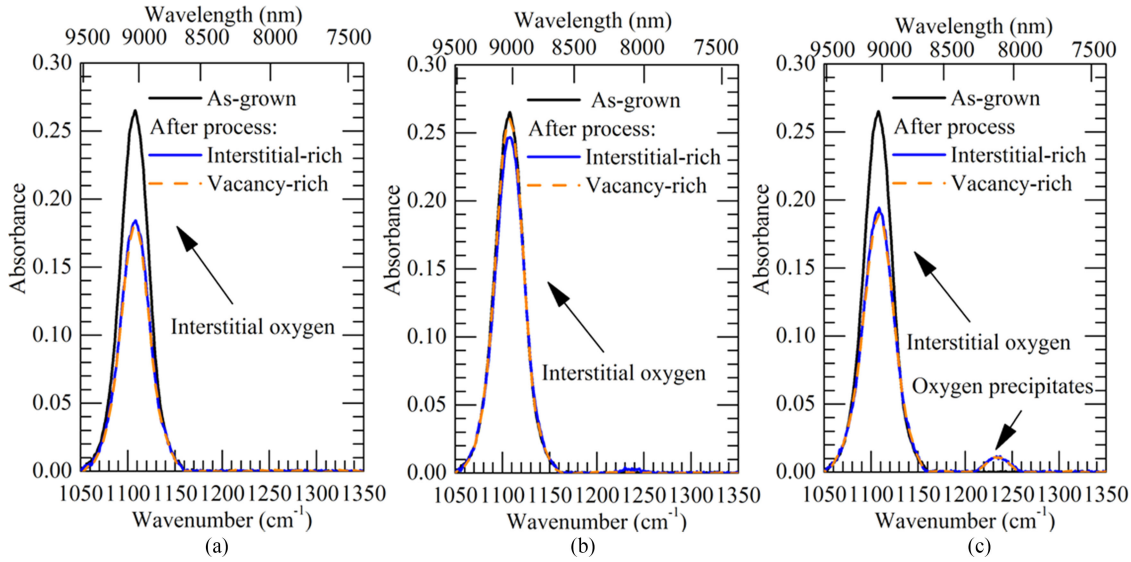

Fig. 4. FTIR spectra in the (a) as-grown slab, (b) oxygen pre-annealed slab, and (c) nitrogen pre-annealed slab; after a two-step anneal. The peak at 1107 cm^{-3} is the absorption peak for interstitial oxygen, the peak at $1230\,cm^{-3}$ is the absorption peak for oxygen precipitates.

In the oxygen pre-annealed slab [see Fig. 4(b)], the interstitial oxygen concentration stays almost unchanged after the two-step annealing. This demonstrates that oxygen pre-annealing is effective at preventing oxygen precipitation. However, note that the oxygen reduction is not-measurable in the vacancy-rich region and very small in the interstitial-rich region, hence the FTIR spectra alone do not allow to understand the difference in lifetime shown in Fig. 2.

Both the as-grown slab and the nitrogen pre-annealed slab show a significant and similar reduction of the interstitial oxygen concentration after two-step anneal. However, for the nitrogen annealed wafers, a peak appears at $1230\,cm^{-1}$ corresponding to oxygen precipitates [34], in particular disc-shape oxygen precipitates [35]. It appears that the same amount of oxygen is precipitated in both the as-grown sample and the nitrogen pre-annealed sample, but only the nitrogen sample shows this oxygen precipitate peak. Possible reasons for this will be discussed below.

C. Oxygen Precipitates and Dislocations

Fig. 5 shows the μ-PL spectra in the interstitial-rich and vacancy-rich zone of all slabs. Note the sub-band-gap luminescence peaks labeled D3/D4 reflect the intrinsic properties of dislocations [36]–[38]. On the other hand, the D1/D2 peaks are usually associated with secondary defects or decoration around oxygen precipitates and dislocations in silicon, which are generally highly recombination active [36]–[38]. In the as-grown slab, the band–band (BB) luminescence intensity is similar after the two-step anneal, which is consistent with the lifetime measurements. The D-lines have low intensity in this sample.

In the oxygen pre-annealed slab, the μ-PL spectra show a much lower BB peak in the interstitial-rich region and a higher band-band peak in the vacancy-rich region, again in agreement with the PL image. The lower BB peak is correlated with high D-lines emissions in the interstitial-rich region, especially D1/D2, which are expected to be recombination active. This suggests that more precipitates and/or dislocations form in the interstitial rich-region of the oxygen annealed slab.

In the nitrogen pre-annealed slab, the μ-PL spectra show a very low BB peak in both the interstitial-rich and vacancy-rich regions. This is also correlated with high D-line peaks in both regions, although D3/D4 are dominant over D1/D2. It seems that a large density of active oxygen precipitates and/or dislocations forms in both regions of the nitrogen annealed slab.

V. Discussion

A. Recombination Activity of Different Precipitate Types

Interestingly, an FTIR oxygen precipitate absorption peak appears at $1230\,cm^{-1}$ in the nitrogen pre-annealed slab. This peak is not present in the slab without pre-annealing whilst both slabs have similar interstitial oxygen reduction.

Two scenarios are possible here: (a) either the concentration of oxygen precipitates is significantly higher in the nitrogen pre-anneal slabs (although the precipitates are smaller accounting for a similar oxygen concentration) leading to the measurable peak at $1230\,cm^{-1}$ and/or (b) the shape of precipitates in the nitrogen annealed sample is different, leading to the absorption peak at $1230\,cm^{-1}$.

Scenarios (a) and (b) could explain why even though the oxygen reduction is similar in the as-grown slabs and the nitrogen annealed slabs, only an oxygen peak is observable in the nitrogen-annealed slabs. The process could be understood as follows: in the nitrogen annealed slab there is a large concentration of vacancies.

1) During the subsequent two-step anneal, it is likely that the high concentration of vacancies (above the critical concentration [13]) leads to a rapid nucleation of precipitates (even at 800 °C) in high concentration. As shown recently [39], the recombination of oxide precipitates depends on their surface area not on their density as previously

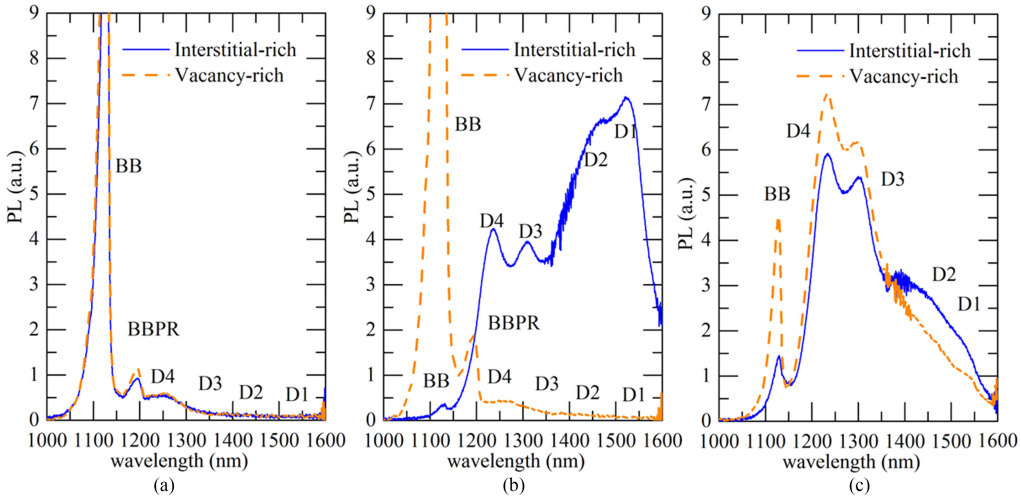

Fig. 5. Microphotoluminescence spectra in the (a) as-grown slab, (b) oxygen pre-annealed slab, and (c) nitrogen pre-annealed slab; after a two-step anneal. BB is the main band-to-band emission assisted by a transverse-optical phonon. BBPR is a phonon replica of the main band-to-band peak (band-to-band emission assisted by a transverse-optical phonon plus an optical zone center phonon). The D lines (D1–D4) are sub-band gap luminescence from dislocations and/or oxygen precipitates.

suggested [2], [4], [5], [9]. Thus, a large amount of smaller precipitates would increase the total surface area of precipitates, leading to a significantly greater reduction of the minority carrier lifetime than in the other slabs.

2) The large vacancy concentration creates a strain leading to the formation of precipitates with high anisotropy (high internal stresses tend to lead to nonspherical oxygen precipitate shape such as plate-like or needle-like). These precipitates are in turn more recombination active than standard spherical precipitates due to their greater surface area [39].

B. Point Defect Concentration Below Critical Concentration in As-Grown State

For the as-grown sample, the fact that precipitation is similar in the interstitial-rich and vacancy-rich region after the two-step anneal could be due to the fact that the vacancy concentration in the vacancy-rich region of the ingot is below the critical concentration necessary to promote precipitate nucleation and/or growth. This is even more likely considering that the vacancy concentration in the middle region is significantly lower than the frozen-in vacancy concentration from the high temperature during ingot cooldown. The vacancy concentration is instead the residual vacancy concentration after vacancy consumption by voids [3], [13]. Note that if this experiment had included a nucleation step at, e.g., 600 °C, precipitate nucleation would have dominated and perhaps lead to a more asymmetric result between the vacancy-rich and interstitial-rich regions of the as-grown wafer [24]. However, such a nucleation step is less relevant for standard solar cell diffusion processes (above 800 °C).

C. Equilibrium Point Defect Concentration During Cooldown of Tabula Rasa Treatment

Tabula rasa or homogenization treatments dissolve grown-in oxygen precipitates that are harmful to the minority carrier lifetime. The higher the temperature at which the treatment is performed (>1000 °C) the smaller the fraction of remaining oxygen precipitates.

However, it is critical that a successful tabula rasa treatment not only dissolves oxygen precipitates but also leads to a low concentration of intrinsic point defects. During tabula rasa cool-down, two processes compete: direct vacancy-interstitial recombination and surface recombination/generation [14]. Silicon self-interstitials are orders of magnitude more mobile than vacancies. Hence in a surface dominated recombination mechanism, the equilibrium point defect concentration is reached faster for an interstitial-rich mode rather than a vacancy-rich mode.

Regarding the pre-oxidized sample, it is clear that the injection of self-interstitials during the oxidation has successfully disabled the growth of oxygen precipitates during the drift phase. However, the large concentration of dislocations after the two-step anneal suggests that the self-interstitial concentration during cooldown from the tabula rasa treatment is above equilibrium in our experiment, especially in the interstitial-rich region. If the interstitial-induced dislocations limit the minority carrier lifetime, this could mean that the cooldown rate ($\sim 20\,\mathrm{K/min}$) is too fast and/or that the surface generation rate of self-interstitials is too high.

As expected, a nitrogen anneal does not disable oxygen precipitation, which is evident in the FTIR interstitial oxygen peak reduction, the oxygen precipitate peak, and the D1 and D2 luminescence lines. This confirms that low equilibrium vacancy concentrations cannot be reached during cooldown of tabula rasa treatment in a nitrogen ambient.

VI. Conclusion

In conclusion, we show that for a similar degree of oxygen reduction, precipitates grown in a vacancy-rich environment (induced by anneal in nitrogen ambient) are more recombination active, or present in higher concentrations, with a negative

impact on the lifetime than for an interstitial-rich environment (induced by anneal in oxygen ambient). We confirm that for intrinsic point defect concentrations below a critical concentration, oxygen precipitation, and dislocation formation are not affected by intrinsic point defects. Finally, our results indicate that in our particular process, nonequilibrium intrinsic point defect concentrations may be created during anneal and cooldown from the tabula rasa treatment with a negative impact on the lifetime upon subsequent processing. More experiments are needed to understand the impact of precipitates and dislocations morphology on their recombination activity.

ACKNOWLEDGMENT

Responsibility for the views, information, or advice expressed herein is not accepted by the Australian Government.

REFERENCES

[1] V. V. Voronkov and R. Falster, "Vacancy-type microdefect formation in Czochralski silicon," *J. Crystal Growth*, vol. 194, pp. 76–88, 1998.
[2] R. Falster and G. Borionetti, "The application of minority carrier lifetime techniques in modern CZ silicon," in *Recombination Lifetime Measurements in Silicon*, ASTM STP 1340, D. C. Gupta, F. Bacher, and W. H. Hughes, Eds. West Conshohocken, PA, USA: Amer. Soc. for Testing and Materials, 1998.
[3] V. V. Voronkov and R. Falster, "Grown-in microdefects, residual vacancies and oxygen precipitation bands in Czochralski silicon," *J. Crystal Growth*, vol. 204, pp. 462–474, 1999.
[4] K. Bothe, R. J. Falster, and J. D. Murphy, "Room temperature subbandgap photoluminescence from silicon containing oxide precipitates," *Appl. Phys. Lett.*, vol. 101, 2012, Art. no. 032107.
[5] J. D. Murphy, K. Bothe, M. Olmo, V. V. Voronkov, and R. J. Falster, "The effect of oxide precipitates on minority carrier lifetime in p-type silicon," *J. Appl. Phys.*, vol. 110, 2011, Art. no. 053713.
[6] J. Haunschild, I. E. Reis, J. Geilker, and S. Rein, "Detecting efficiency-limiting defects in Czochralski-grown silicon wafers in solar cell production using photoluminescence imaging," *Phys. Status Solidi, Rapid Res. Lett.*, vol. 5, pp. 199–201, 2011.
[7] L. Chen *et al.*, "Effect of oxygen precipitation on the performance of Czochralski silicon solar cells," *Sol. Energy Mater. Sol. Cells*, vol. 95, pp. 3148–3151, 2011.
[8] H. Angelskar, R. Sondena, M. S. Wiig, and E. S. Marstein, "Characterization of oxidation-induced stacking fault rings in Cz silicon: Photoluminescence imaging and visual inspection after wright etch," *Energy Procedia*, vol. 27, pp. 160–166, 2012.
[9] J. D. Murphy, K. Bothe, R. Krain, V. V. Voronkov, and R. J. Falster, "Parameterisation of injection-dependent lifetime measurements in semiconductors in terms of Shockley-Read-Hall statistics: An application to oxide precipitates in silicon," *J. Appl. Phys.*, vol. 111, 2012, Art. no. 113709.
[10] L. Peidong *et al.*, "The influencing factors and formation mechanism of the dark ring of monocrystal silicon cells," in *Proc. Semicond. Technol. Int. Conf.*, 2015, pp. 1–3.
[11] G. Gaspar *et al.*, "Identification of defects causing performance degradation of high temperature n-type Czochralski silicon bifacial solar cells," *Sol. Energy Mater. Sol. Cells*, vol. 153, pp. 31–43, 2016.
[12] R. J. Falster *et al.*, "Vacancy-assisted oxygen precipitation phenomena in Si," *Solid State Phenom.*, vol. 57-58, pp. 129–136 1997.
[13] V. V. Voronkov and R. Falster, "Effect of vacancies on nucleation of oxide precipitates in silicon," *Mater. Sci. Semicond. Process.*, vol. 5, pp. 387–390, 2002.
[14] R. Falster and V. V. Voronkov, "The engineering of intrinsic point defects in silicon wafers and crystals," *Mater. Sci. Eng. B*, vol. 73, pp. 87–94, 2000.
[15] W. Wijaranakula, "Effect of point defect reactions on behavior of boron and oxygen in degenerately doped Czochralski silicon," *Appl. Phys. Lett.*, vol. 62, pp. 2974–2976, 1993.
[16] M. Pagani, R. J. Falster, G. R. Fisher, G. C. Ferrero, and M. Olmo, "Spatial variations in oxygen precipitation in silicon after high temperature rapid thermal annealing," *Appl. Phys. Lett.*, vol. 70, pp. 1572–1574, 1997.
[17] A. Sarikov *et al.*, "Mechanisms of oxygen precipitation in Cz-Si wafers subjected to rapid thermal anneals," *J. Electrochem. Soc.*, vol. 158, pp. H772–H777, 2011.
[18] C. Cui, D. Yang, X. Ma, R. Fan, and D. Que, "Effect of annealing atmosphere on oxygen precipitation and formation of denuded zone in Czochralski silicon wafer," *Phys. Status Solidi A*, vol. 203, pp. 2370–2375, 2006.
[19] V. V. Voronkov, R. Falster, T. Kim, S. Park, and T. Torack, "Depth profiles of oxygen precipitates in nitride-coated silicon wafers subjected to rapid thermal annealing," *J. Appl. Phys.*, vol. 114, 2013, Art. no. 043520.
[20] W. J. Taylor, T. Y. Tan, and U. M. Gösele, "Oxygen precipitation in silicon: The role of strain and self-interstitials," *Appl. Phys. Lett.*, vol. 59, pp. 2007–2009, 1991.
[21] L. Mule'Stagno, "A technique for delineating defects in silicon," in *Proc. Gettering Defect Eng. Semicond. Technol. IX*, 2001, pp. 753–758.
[22] K. H. Yang, "A preferential Etch for silicon crystals," in *Proceeding of Semiconductor Processing*, ASTM STP 850, D. C. Gupta, Ed. West Conshohocken, PA, USA: Amer. Soc. for Testing and Materials, 1984.
[23] K. H. Yang, "An etch for delineation of defects in silicon," *J. Electrochem. Soc.*, vol. 131, pp. 1140–1145, 1984.
[24] R. J. Falster, M. Cornara, D. Gambaro, M. Olmo, and M. Pagani, "Effect of high temperature pre-anneal on oxygen precipitates nucleation kinetics in Si," *Solid State Phenom.*, vol. 57–58, pp. 123–128, 1997.
[25] K. F. Kelton *et al.*, "Oxygen precipitation in silicon: Experimental studies and theoretical investigations within the classical theory of nucleation," *J. Appl. Phys.*, vol. 85, pp. 8097–8111, 1999.
[26] C. A. Londos, M. S. Potsidi, and V. V. Emtsev, "Effect of carbon on oxygen precipitation in Czochralski silicon," *Phys. Status Solidi C*, vol. 2, pp. 1963–1967, 2005.
[27] T. Trupke, R. A. Bardos, M. C. Schubert, and W. Warta, "Photoluminescence imaging of silicon wafers," *Appl. Phys. Lett.*, vol. 89, 2006, Art. no. 044107.
[28] R. A. Sinton and A. Cuevas, "Contactless determination of current-voltage characteristics and minority-carrier lifetimes in semiconductors from quasi-steady-state photoconductance data," *Appl. Phys. Lett.*, vol. 69, pp. 2510–2512, 1996.
[29] C. Schinke *et al.*, "Uncertainty analysis for the coefficient of band-to-band absorption of crystalline silicon," *AIP Adv.*, vol. 5, 2015, Art. no. 067168.
[30] F. Schindler *et al.*, "Material limits of multicrystalline silicon from state-of-the-art photoluminescence imaging techniques," *Prog. Photovolt.: Res. Appl.*, to be published.
[31] J. A. Giesecke, R. A. Sinton, M. C. Schubert, S. Riepe, and W. Warta, "Determination of bulk lifetime and surface recombination velocity of silicon ingots from dynamic photoluminescence," *IEEE J. Photovolt.*, vol. 3, no. 4, pp. 1311–1318, Oct. 2013.
[32] S. Bowden and R. A. Sinton, "Determining lifetime in silicon blocks and wafers with accurate expressions for carrier density," *J. Appl. Phys.*, vol. 102, 2007, Art. no. 124501.
[33] A. Cuevas, "Modelling silicon characterisation," *Energy Procedia*, vol. 8, pp. 94–99, 2011.
[34] A. Borghesi, A. Piaggi, A. Sassella, A. Stella, and B. Pivac, "Infrared study of oxygen precipitate composition in silicon," *Phys. Rev. B*, vol. 46, pp. 4123–4127, 1992.
[35] B. Pivac, A. Borghesi, M. Geddo, A. Sassella, and A. Stella, "Stoichiometry of oxygen precipitates in silicon," *Appl. Surf. Sci.*, vol. 63, pp. 245–248, 1993.
[36] S. Binetti *et al.*, "Optical properties of oxygen precipitates and dislocations in silicon," *J. Appl. Phys.*, vol. 92, pp. 2437–2445, 2002.
[37] E. A. Steinman, A. N. Tereshchenko, V. Y. Reznik, and R. J. Falster, "Radiative properties of dislocations generated around oxygen precipitates in Si," *Physica Status Solidi A*, vol. 204, pp. 2238–2247, 2007.
[38] M. Tajima *et al.*, "Deep-level photoluminescence due to dislocations and oxygen precipitates in multicrystalline Si," *J. Appl. Phys.*, vol. 111, 2012, Art. no. 113523.
[39] J. D. Murphy *et al.*, "The effect of oxide precipitates on minority carrier lifetime in n-type silicon," *J. Appl. Phys.*, vol. 118, 2015, Art. no. 215706.

Authors' photographs and biographies not available at the time of publication.